International Journal of Heat and Fluid Flow 30 (2009) 369–379

Contents lists available at ScienceDirect

International Journal of Heat and Fluid Flow

journal homepage: www.elsevier.com/locate/ijhff

An experimental investigation of pneumatic swirl flow induced by a three lobed helical pipe

S. Fokeer [a,*], I. Lowndes [b], S. Kingman [b]

[a] Department of Aeronautical and Automotive Engineering, University of Loughborough LE11 3TU, UK
[b] Division of Process and Environmental Engineering, University of Nottingham, Nottingham NG7 2RD, UK

ARTICLE INFO

Article history:
Received 22 February 2008
Received in revised form 7 November 2008
Accepted 9 December 2008
Available online 20 January 2009

Keywords:
Swirl induction
Laser Doppler Anemometry
Wall jet swirl
Swirl number
Swirl decay

ABSTRACT

This paper presents a discussion of the results and conclusions drawn from a series of experiments conducted to investigate the swirl flow that are generated by a three lobed helical pipe mounted within a laboratory scale pneumatic conveying rig. The experiments employed Laser Doppler Anemometry (LDA) to quantify the strength of the induced vortex formations and the decay rates of the observed downstream swirl flows over a range of Reynolds number in the turbulent regime. Instantaneous point velocity measurements were resolved in three directions across regular measurement grids transcribed across parallel planes located at four distances downstream of the swirl inducing pipe section. The equivalent axial, radial and tangential velocities were subsequently computed at these grids points. The degree of swirl measured across each measurement plane was expressed in terms of a defined swirl number.

It was concluded that the three lobed helical pipe gave rise to a wall jet type of swirl whose rate of observed downstream decay is related to the Reynolds number of the upstream flow and the distance downstream of the swirl pipe. The decay rates for the swirl flows were found to be inversely proportional to the Reynolds number of the upstream flow. The swirl pipe was observed to create a redistribution of the downstream velocity field from axial to tangential, accompanied by a transfer of axial to angular momentum. The findings of this paper are believed to improve understanding to assist the selective use of swirl flow within lean phase particles pneumatic transport systems.

1. Introduction

This paper presents the results of a series of experiments performed to study the downstream flow regimes created by the insertion of a three lobed helical pipe within a pneumatic flow system. Lean phase pneumatic conveying is widely used to transport suspended solid particulate materials, with particle sizes ranging from tens of microns to tens of centimetres, in a confined gas stream. The major challenges faced by pneumatic conveying systems are: the identification and maintenance of the correct conveying velocity to avoid segregation and material blockages; the optimisation of the maximum conveying velocity to reduce the resultant high pressure loss and operating costs and pipe wear (Tashiro et al., 1997; Jama et al., 1999; Herbreteau and Bouard, 2000). For a review of lean phase pneumatic flows and the associated problems, see Fokeer et al. (2004). The results of recent experimental studies have suggested that a partial solution to these problems may be achieved by locally increasing the conveying velocity within a pneumatic circuit (Li and Tomita, 2000), following an enlargement in the pipeline cross sectional area or prior to a bend in the pipeline. A practical method to locally increase the conveying velocity is to increase the turbulence of the conveying fluid by imparting a swirling motion to the flow (Chang and Dhir, 1995; Li and Tomita, 2000; Ganeshalingam, 2002). There are a number of potential swirl flow devices that have been studied by previous researchers. These include: propeller type swirl generators (Zaherzadeh and Jagadish, 1975; Bali and Ayhan, 1999), tangential slots (Hay and West, 1975), honeycomb structures (Nishibori et al., 1987), and inserts of twisted tapes, wires or tubes mounted within the inlet to a pipe section (Narezhnyi and Sudarev, 1975; Algifri and Bhardwaj, 1985).

1.1. The anatomy of swirl flows

Kitoh (1991) and Martemianov and Okulov (2004) have suggested that the method of swirl generation can play an important role in the production of different types of swirl and axial vorticity profiles. Nevertheless, the basic characteristics of a swirling flow are a combination of primary and secondary flows. The primary flow component being parallel to the downstream flow direction, and the secondary flow component being a circulatory fluid motion about the axes of symmetry of the pipe, parallel to the primary flow (Chiu and Seman, 1971). The combination of these two flows

* Corresponding author. Tel.: +44 0 7872114710; fax: +44 0 150 922 7275.
E-mail address: S.Fokeer@lboro.ac.uk (S. Fokeer).

0142-727X/$ - see front matter © 2008 Elsevier Inc. All rights reserved.
doi:10.1016/j.ijheatfluidflow.2008.12.004

Nomenclature

u	mean velocity in the x-direction (ms^{-1})	x	distance in x-direction (m)
v	mean velocity in the y-direction (ms^{-1})	r	radial distance from pipe centreline (m)
w	mean velocity in the z-direction (ms^{-1})	D	pipe radius (m)
u_x	mean axial velocity (ms^{-1})	S	swirl number or swirl intensity
u_r	mean radial velocity (ms^{-1})	S_0	initial swirl number or intensity
u_θ	mean tangential velocity (ms^{-1})	β	decay rate of swirl intensity

creates a swirl or tangential velocity component to the flow, producing a helical winding of the streamlines that are a characteristic of swirling flows.

The induced swirling flow field will eventually decay with increasing distance downstream and revert back to the upstream flow profile at a few pipe diameters downstream. As this transition occurs the radial location of the maximum tangential velocity moves away from the pipe centreline, i.e., the core region shrinks as swirl decays, as predicted by the Rankine vortex-based model (Algifri et al., 1988; Bali, 1998). During swirl decay, the magnitudes of the turbulence intensities were observed to sharply decrease at the core, whilst only a slight change was observed closer to the wall (Algifri et al., 1988). The velocity gradient of the tangential velocity component was observed to gradually deform into a concave profile (Nishibori et al., 1987).

Li and Tomita (1996, 1998) and Li et al. (1999) have recently conducted experimental investigations to study the application of swirl flows to horizontal pneumatic conveying (Swirl Flow Pneumatic Conveying). An analysis of the results of these studies concluded that the application of swirl could: lower the critical and minimum conveying velocities, the pressure drops, the fluctuations in the wall static pressure, and the power consumption as compared to the equivalent experimental rigs employing conventional axial flow pneumatic conveying. Furthermore, the particle concentration profiles were found to be symmetrically distributed with respect to the pipe axis. It was concluded that the dominating micro-physical transport phenomena in swirl flow pneumatic conveying were: the turbulent transport of particles, particle-wall collisions and inter-particle collisions. These encouraging findings promoted the execution of the lean phase pneumatic swirl flow experimental studies that form the basis of this paper. The swirl intensity or swirl number, S, is commonly used to quantify the degree or the strength of a swirl within a pipe. This non-dimensional number is defined as the ratio of the swirl/angular momentum flux to the axial momentum flux, multiplied by the hydraulic radius (Kitoh, 1991). A widely accepted simplification of the swirl number is given by the following formula (Rocklage-Marliani et al., 2003):

$$S = \frac{\int_0^R u_x u_\theta r^2 dr}{D \int_0^R u_x^2 r dr} \tag{1}$$

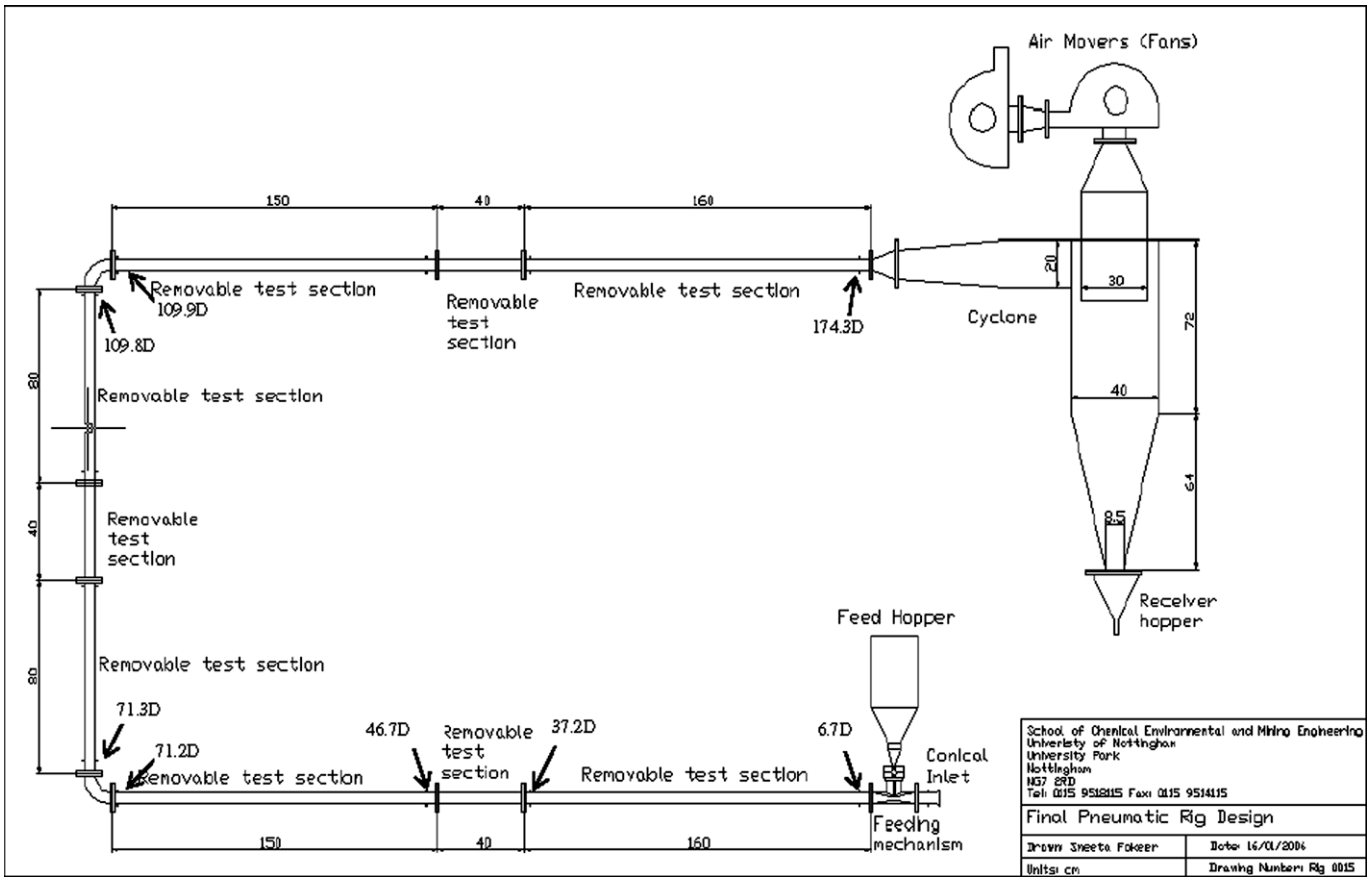

Fig. 1. Schematic illustration of pneumatic conveying rig.

Parchen and Steenbergen (1998) have shown that the swirl intensity, defined by Eq. (1), is observed to follow an exponential decay of the form:

$$S = S_0 e^{-\frac{\beta x}{D}} \tag{2}$$

where β is the decay rate, S_0 is the initial swirl intensity, x is the axial distance downstream of the swirl inducing pipe section and D is the pipe diameter.

2. Experimental objectives and methodology

The primary aim of the experimental study reported in this paper was to investigate the flow regime created downstream of a three lobed helical pipe placed within in a horizontal pipe section. The specific objectives were: to characterise these flow by mapping the velocity distributions, to quantifying the vortex formation and swirl decay rates for a range of turbulent air flow rates.

A number of recent experimental studies (Parchen and Steenbergen, 1998; Nejad et al., 1989; Rocklage-Marliani et al., 2003) have demonstrated that Laser Doppler Anemometry (LDA) can be successfully employed to study swirl flows. The major disadvantages of the application of LDA techniques are that they need an optically transparent flow conduit and flow field through which the light beams can pass, that they do not give continuous velocity signals and they require the use of light-scattering tracer particles suspended in the flow. Since, it is the velocity of the particles that is measured, the relationship between the particle velocity and that of the fluid must be known. To make this problem tractable, it is important to ensure that the particle sizes and concentrations are small enough to be insignificant i.e. the Stokes Number, $St < 1$.

Consequently, LDA was employed to measure the instantaneous velocities of the flow field downstream of the swirl-inducing pipe. Due to the limitations that the LDA technique imposes on the size of the seeded particles within the flow, the LDA experiments were carried out using an air only flow. The flow was seeded with oil droplets of an average diameter of 3 μm by a generator located upstream of the swirl inducing pie section. From the flow field characteristics that are revealed as a result of the experiments, the assumption is that the influence of such a swirling flow on the fully suspended particles' paths and cross sectional distribution during lean phase pneumatic conveying can be inferred from the flow field as long as the particles are assumed to be neutrally buoyant. This assumption will limit the practical size range of the particles to which the experimental results will be applicable.

2.1. Description of the experimental rig

The experimental study was carried out on a specially constructed laboratory scale pneumatic conveying rig. The rig was constructed out of clear 50 mm internal diameter Perspex tubing with a horizontal flow section of high optical quality quartz glass inserted downstream of the swirl flow section to enable LDA measurements to be made. The rig consisted of a lower 3.5 m horizontal flow section with a calibrated inlet cone, a 90° horizontal to vertical bend leading to a 2 m vertical riser section, a 90° vertical to horizontal bend leading to an upper 3.5 m horizontal flow section connected to a 0.4 m diameter cyclone and a set of two series connected 1.8 kW exhaust flow fans. The total flow run of the rig was 9 m (180D), with a maximum horizontal straight of 3.5 m (70D) and a maximum vertical of 2 m (40D). The radius to diameter

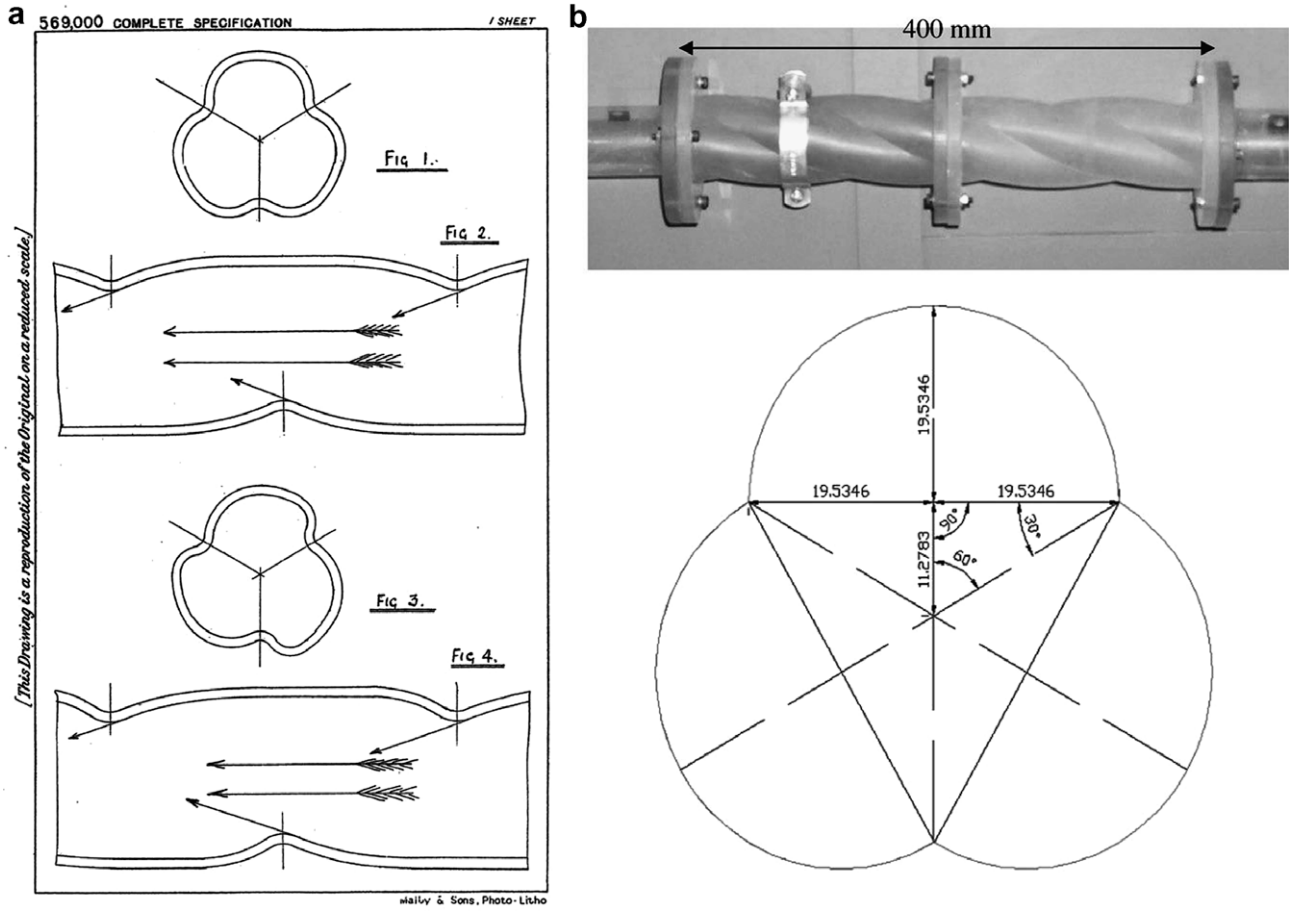

Fig. 2. (a) Patented design of a 3-lobed boiler tube by Spanner (1945); (b) Helical turbulence inducing test pipe geometry (dimensions in mm).

ratio of the bends was 1.9.The 0.4 m length helical turbulence-inducing pipe was placed within the lower horizontal flow pipe 1.9 m (38D) downstream of the inlet cone. A schematic of the rig is shown in Fig. 1. The rig consisted of a conical inlet for air mass flow rate measurements, variable feed gravity hopper, a 0.4 m diameter cyclone and two 1800 W fans in series with variable power. Pressure tappings were included to measure the pressure drop at the specified pipe diameters downstream of the air inlet. The rig was operated as a low negative pressure system.

The operating performance of the rig was established by performing a series of fan tests, rig pressure drop tests for flows of varying Reynolds number, first using a conventional straight pipe and then using the swirl pipe inserted in the lower test section of the rig. The swirl pipe and the 90° bends were confirmed to exhibit an increased pressure drop as compared to a comparable straight length of pipe section.

2.2. Swirl inducing pipe

The use of a helical lobed pipe to induce swirl within a fluid flow was recently investigated by Raylor (1998) and Ganeshalingam (2002) using a similar pipe designed to increase the efficiency of heat exchanger pipes used in marine boilers. This device was patented by Spanner (1945). A series of diagrammatic representations of the three lobed helical pipe section are shown in Fig. 2a. Raylor (1998) and Ganeshalingam (2002) later showed that that a near-optimum design for such a device applied to hydraulic conveying consisted of a lobed geometry of fixed cross-section and constant helix. Hence a 0.4 m length of 3-lobe cross-section pipe with average diameter 0.05 m, and a helical pitch of 0.3 m was used for the swirl inducing pipe. The pitch of the swirl inducing pipe is 30 cm (6 D). The cross sectional geometry and a picture of the swirl inducing pipe is shown in Fig. 2b.

2.3. Velocity measurements

Velocities were measured within the pneumatic swirl flow rig using a DANTEC Flowlite 1D LDA system. The device consists of a Fibre Flow Probe, fibre-optic cable, an optics unit and Burst Spectrum Analyser (BSA) enhanced signal processor. The system employs a 10 mW Helium Neon laser which produces red light of wavelength 632.8 nm. A Bragg cell, which shifts the frequency of one of the beams by 40 MHz is used to resolve negative velocities from positive velocities. The positive velocity was defined in the downstream direction.

Thus the length of the measuring volume along the optical axis was approximately 1.7% of the pipe diameter and considerably less in the other two directions giving adequate spatial resolution for the measurement of velocity profile.

Stream wise, span wise and plane wise velocity components were measured by re-orientating the laser probe onto a 2D traverse gear. The pneumatic flow was artificially seeded using white Shell Ondina oil smoke produced by an SPT smoke generator (model 90) and delivered through a straight probe located upstream of the calibrated inlet cone. The smoke fluid has a specific gravity of 0.835 and generated particles of a nominal diameter of 1.5 μm.

The major operating parameters of the LDA system used are summarized in Table 1.

Preliminary experiments established that repeatable and accurate readings could be taken up to $r/D = 0.92$ in the y-direction and 0.88 in the z-direction for both the horizontal and vertical beams. A measurement matrix, constituting of coordinates of 130 measurement points over the pipe cross sectional area of 1963.5 mm^2, was derived to cover the maximum possible cross sectional area of the downstream optical pipe section. This measurement grid was used to direct the traverse system to these exact measurement locations as shown in Fig. 8a.

The laser beam and detection system were optimised to obtain the best possible amplitude, volume and regularity of the fringe pattern. In the measurement of all three velocity components, the LDA signal was filtered with a band pass filter (1–12 kHz) to reduce the noise level of the transmitted signal and to eliminate the signal pedestal. The flow configurations envisaged for the experimental study were determined to create Doppler signals with frequencies varying from 3.73 to 11.18 kHz. The maximum number of data samples to be taken per measurement location was pre-specified to be 2500 and the measurement time set as 20 s per location. Measurement was considered complete if either of these two conditions was satisfied. During the measurement cycle, the LDA sig-

Table 1
Main operating parameters of LDA system.

LDA system parameter		Value
Focal length	f (mm)	160
Beam separation at converging lens	D_b (mm)	38
Fringe spacing	d_f (m)	2.68
Beam diameter at converging lens	D_l (mm)	0.099
Length of measurement volume in x-direction	l_m (mm)	0.840
Length of measurement volume in y-direction	d_m (mm)	0.130
Length of measurement volume in z-direction	h_m (mm)	0.099
Volume of measurement volume	V_d (mm^3)	0.0043

Table 2
Experimental conditions at inlet.

	Conditions at inlet		
	Mean air mass flowrate (kg/s)	Mean velocity (m/s)	Reynolds number
Low	0.024 ± 0.00169	10 ± 0.015	4.5 × 104 ± 791
Medium	0.047 ± 0.00086	20 ± 0.016	9.0 × 104 ± 404
High	0.071 ± 0.00057	30 ± 0.019	1.4 × 105 ± 269

Table 3
Summary of measurement strategy.

		Low Reynolds number flow			Medium Reynolds number flow			High Reynolds number flow		
		u vel	v vel	w vel	u vel	v vel	w vel	u vel	v vel	w vel
Swirl pipe	2D	Plane	Plane	Plane	Plane	Plane	Plane	Plane	Plane	Plane
	6D	Plane	Plane	Plane	Plane	Plane	Plane	Plane	Plane	Plane
	10D	Plane	Plane	Plane	Plane	Plane	Plane	Plane	Plane	Plane
	14D	Plane		Line	Plane		Line	Plane		Line
Control pipe	2D	Plane		Line	Plane		Line	Plane		Line
	6D	Plane		Line	Plane		Line	Plane		Line
	10D	Plane		Line	Plane		Line	Plane		Line
	14D	Plane		Line	Plane		Line	Plane		Line

nal burst was manually monitored to reduce noise and ensure that the spectrum was always centred and bell-shaped. The high voltages of the photomultiplier and signal gain were adjusted to get a high data rate with an acceptance rate of about 80%. However this was not always possible due to reflections, local glass pipe quality and dust on the glass.

2.4. Measurement programme

The experimental programme was set to measure the velocity components at four different planes within an optical pipe section perpendicular to the downstream flow direction for three different turbulent flow regimes summarised in Table 2.

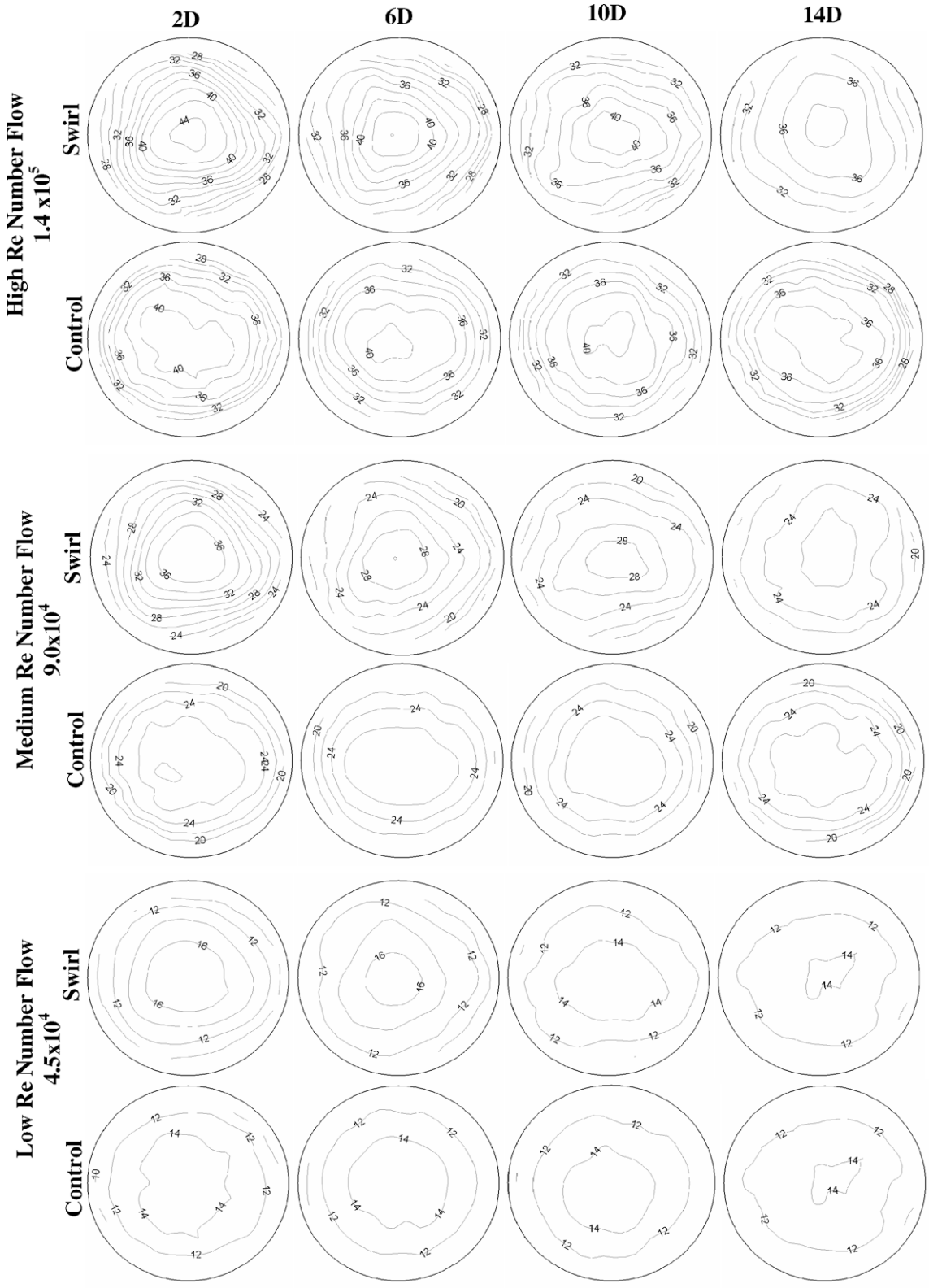

Fig. 3. Comparison of axial air velocity contours downstream of the swirl and control pipe for low, medium and high Reynolds number flows.

The measurement plane locations were at 2, 6, 10 and 14 pipe diameters downstream of the control and swirl pipe sections outlet. Full sets of the three orthogonal flow velocities (u, v and w) were recorded at the measurement points defined in Fig. 8a for planes 2D, 6D and 10D downstream of the swirl pipe. As the swirl from preliminary experiments had been observed to have decayed within 14 pipe diameters downstream of the outlet of the swirl pipe, the u velocity was measured at all the measurement points defined in Fig. 8a, while w velocity was measured at 25 points along a single horizontal diameter of the pipe, extending between $r/D = \pm 0.92$. The same measurement strategy was employed for the experiments performed with the conventional straight control pipe test section. Table 3 summarises the measurement matrix employed.

2.5. Data transformation

The raw individual LDA data files reported x, y and z coordinates, the mean velocity, the root mean square (rms) value of the velocity and turbulence intensity. Velocity data with an rms value of 10 or greater was considered as erroneous and was substituted with value interpolated from its neighbouring data points. A total of ten substitutions were made in total. These tended to occur close to the pipe wall in the high and low z regions due to the high curvature of the pipe wall experienced by the laser beams as they pass through the glass pipe wall.

The experimental velocity measurements were determined using a Cartesian frame of reference. The measured Cartesian velocity components were converted into cylindrical velocity components using the conventional transformations detailed below:

$$u = u \tag{3a}$$

$$u_r = v\cos\theta + w\sin\theta \tag{3b}$$

$$u_\theta = w\cos\theta - v\sin\theta \tag{3c}$$

The data was plotted as a 2D plot of y-values against z values. A regular 23 mm diameter circular mesh was created with 20 cells in the radial direction and 50 in the circumferential direction to encompass the area covered by the data. The data was then interpolated on this mesh using the kriging technique described by Davis (1986). The resultant axial, radial and tangential velocity contours were then plotted and are shown on the following sections. Axial velocity contours were plotted to a uniform scale to show a velocity range of 0–50 m/s.

3. Analysis and discussion of the experimental data

3.1. Axial velocity for swirl inducing and control pipe

The contour plots of the axial velocities computed for the three Reynolds number flows downstream of the control and swirl induced pipe are shown in Fig. 3. In both the straight control and swirl pipe experiments, the cross sectional axial velocity distributions reflected the Reynolds number of the flow; with the higher velocities recorded for the higher Reynolds number flows and lower velocities recorded at the lower Reynolds number flows. The centreline velocity was observed to decrease with increasing distance downstream for all flows. Similarly, low velocities were observed closer to the wall, increasing to a maximum at the centre of the pipe for all of the flow regimes.

The main striking feature observed from an examination of these plots is the more three sided nature of the velocity contours observed for the swirl induced flows as opposed to the more circular shaped ones determined for the conventional straight test section control flows. It is concluded that this three sided velocity contour is created by the 3-lobed helical swirl pipe, whereby each vertices of the triangular shape is caused by one of the lobe of the helical tube. The triangular shape is most distinct closer to the exit of the swirl pipe and fades with increasing distance downstream.

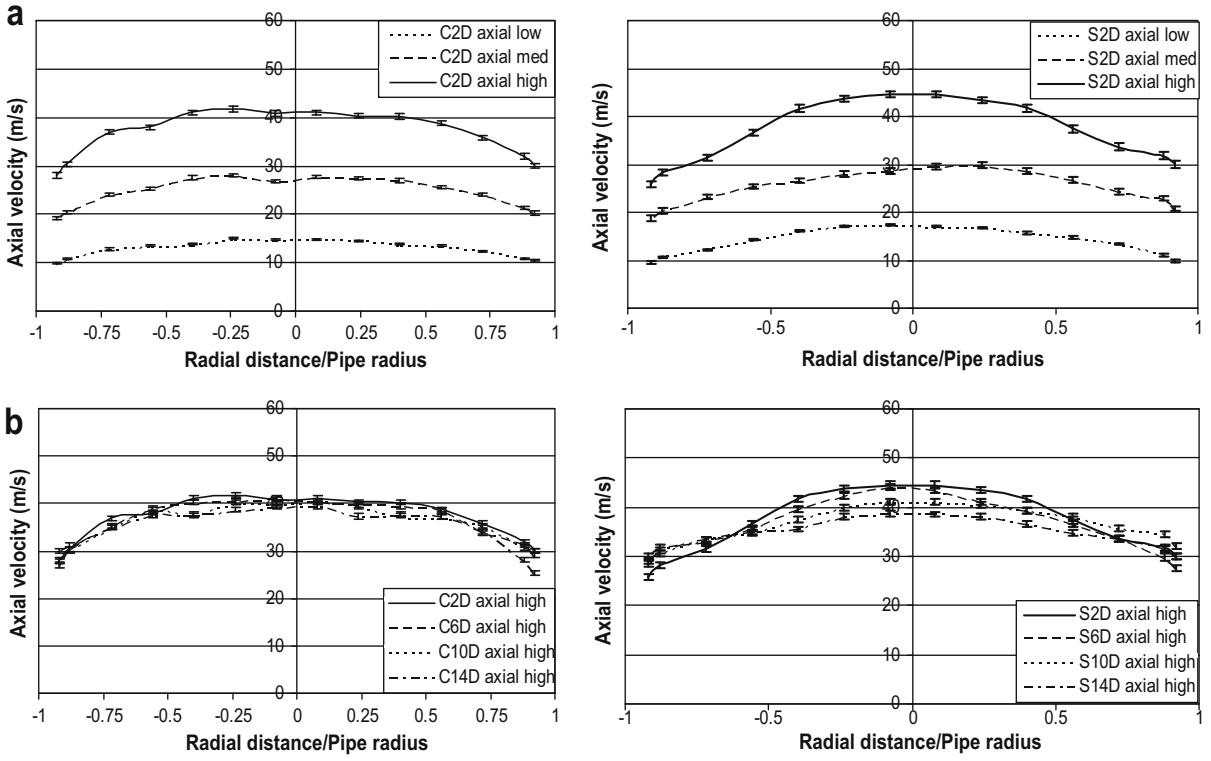

Fig. 4. (a) Axial air velocity along the horizontal centreline of the pipe at plane 2D downstream of the control and swirl inducing pipe at low, medium and high Reynolds number flows; (b) axial velocity along the horizontal centreline of the pipe at planes 2D, 6D, 10D.

However, remnants of the triangular shape of the velocity contours were observed to persist up to 14 pipe diameters downstream of the outlet of the swirl pipe. It is observed that the triangular shaped contours are better sustained at high Reynolds number flows despite increasing distance downstream of the swirl pipe. The orientation of the triangular contours shifted with increasing distance downstream of the swirl pipe as it reflects a rotating flow.

The pitch of the swirl inducing pipe is 30 cm (6D). If the flow follows the geometry of the swirl pipe closely and continues to do so downstream of the swirl pipe, the triangular contours would have been offset by 120°, 0°, 240° and 120° (with reference with the positive x-axis) at 2, 6, 10 and 14 pipe diameters respectively downstream of the swirl pipe. With the exception of the contour orientation at 2D, this was not observed. It was therefore concluded that as the Reynolds number of the flow increases the induced swirl decays with increasing distance downstream of the swirl pipe.

These findings were subsequently confirmed by an analysis of the computed axial flow velocities plotted in Fig. 3. Fig. 4 shows a plot of 14 axial velocity measurements along the horizontal centreline of the pipe at plane 2D downstream of the control and swirl inducing pipe at low, medium and high Reynolds number flows and at planes 2, 6, 10 and 14D downstream of the outlet of the control and swirl inducing pipe sections at high Reynolds number flows. The combined percentage error from the LDA measurements and fan fluctuations were estimated to vary from 1.51% to 2.01% for the cases reported in Fig. 4.

It was observed that the downstream velocity gradient at the centre of the pipe for all three flows regimes for the control pipe, and the medium and low Reynolds number flows for the swirl pipe, were almost flat, indicating that all the flows were turbulent, even at the furthest downstream location measured.

However, for the high Reynolds number flow, a sudden increase in the axial velocity was observed at $r/D \approx \pm 0.5$. This trend was observed at two and six pipe diameters downstream of the swirl pipe, but faded away further downstream. It was concluded that this higher core velocity was created by the swirl flow induced by the swirl pipe section.

3.2. Radial and tangential velocity for swirl inducing pipe

An analysis of the radial velocity contours shown in Fig. 5 identified alternate pairs of radial velocity high-spots and low-spots across the pipe cross sections for the range of flow regimes tested. These high-spots were more evident at the high Reynolds number flow and at diameters closer to the exit of the swirl pipe section. It was concluded that the position of these high–low radial velocity pairs corresponded to the vertices of the triangular axial velocity contours described above. The alternative pairs of radial velocity high- and low-spots, as depicted in the pipe cross section at two diameters downstream of the swirl pipe for high Reynolds number flow, could create localised vortices in that plane.

Fig. 6 shows the computed tangential velocity profiles along the horizontal centreline of the measurement planes located at 2, 6, 10 and 14 diameters downstream of the outlet to the straight control

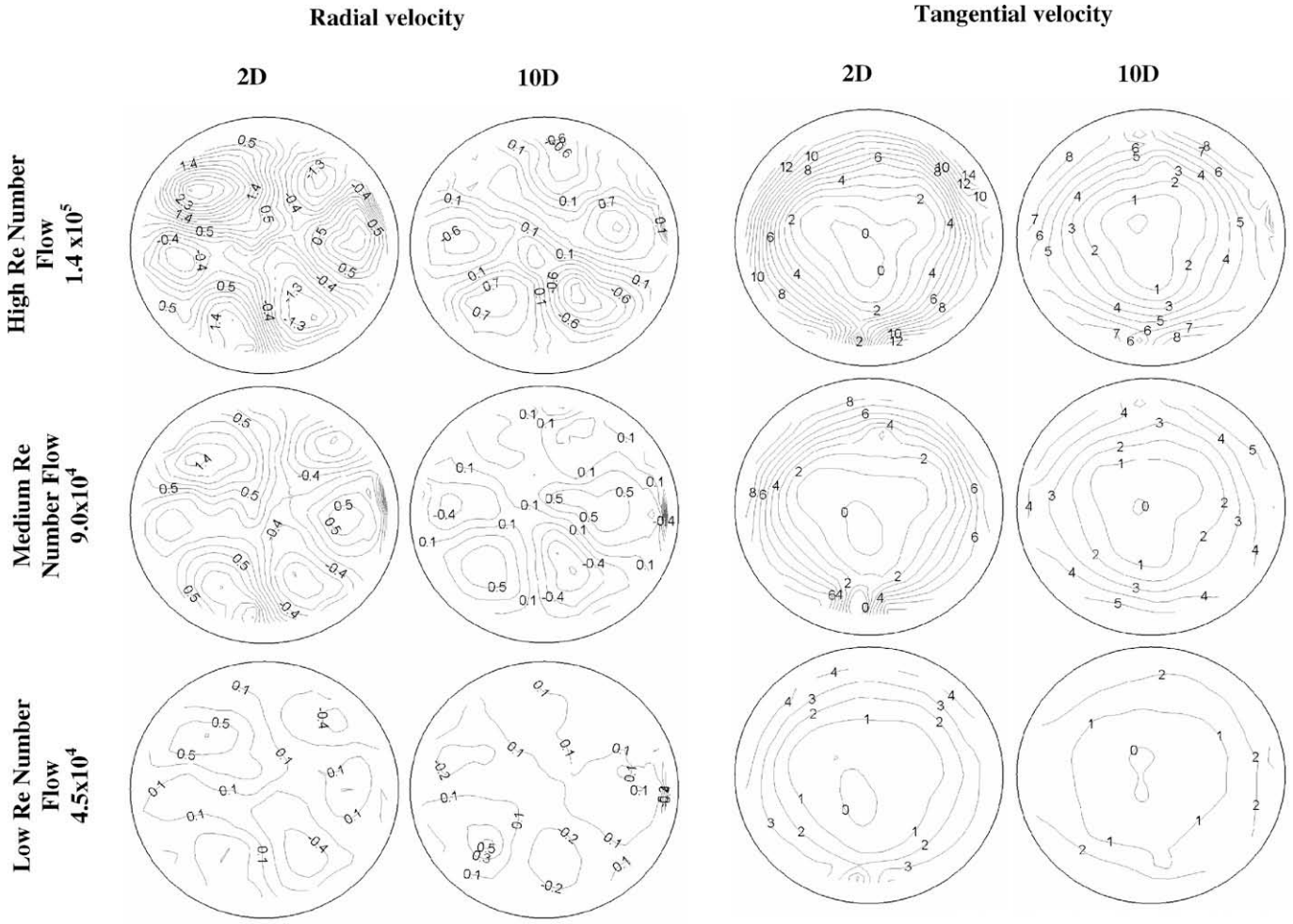

Fig. 5. Radial and tangential air velocity contours at planes 2 and 10 diameters downstream of swirl inducing pipe.

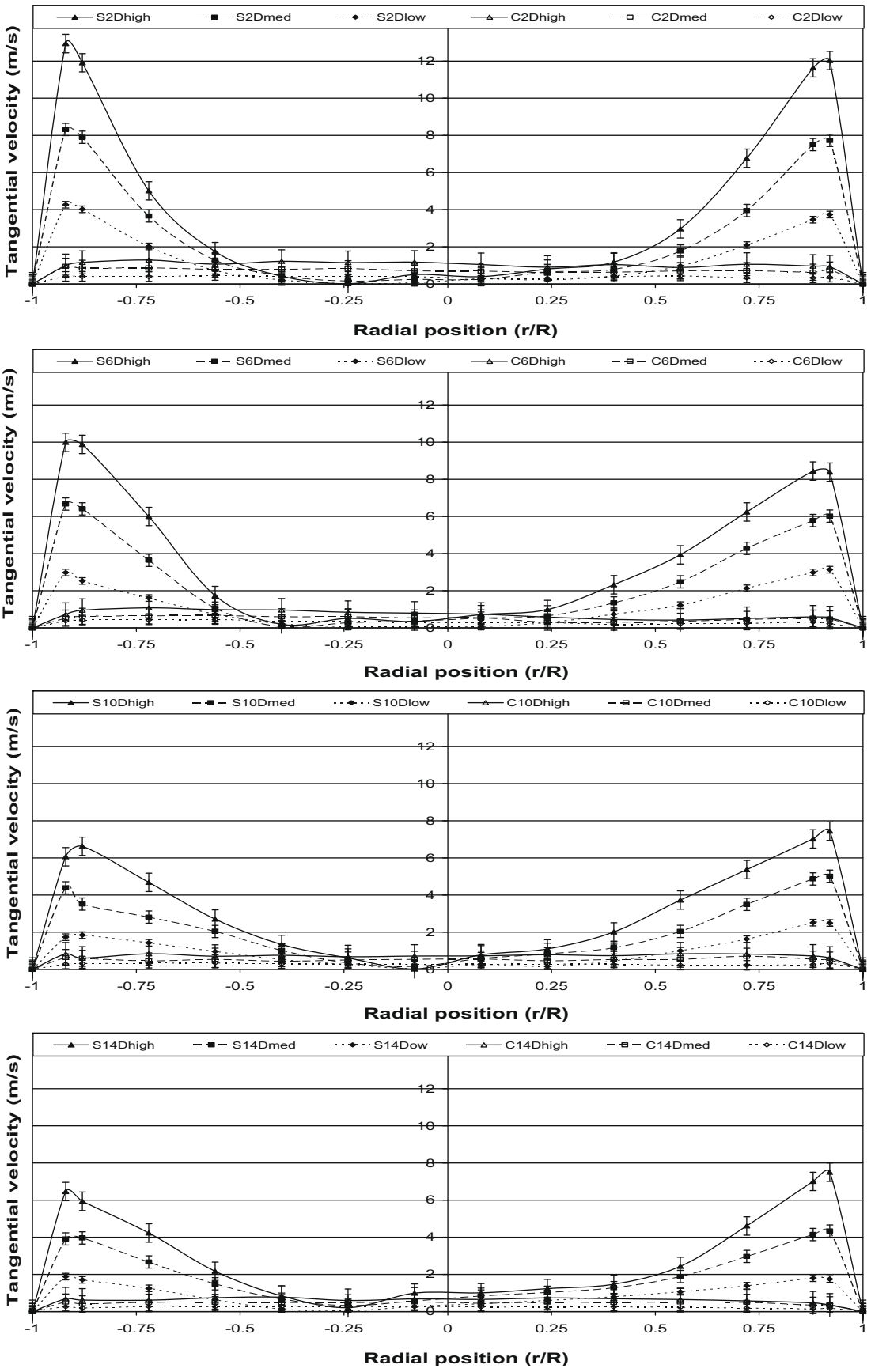

Fig. 6. Tangential air velocity profiles downstream of the swirl and control pipe sections for all three values of turbulent Reynolds number flow regimes tested (all measurements were taken across the horizontal internal pipe diameter of each measurement cross section).

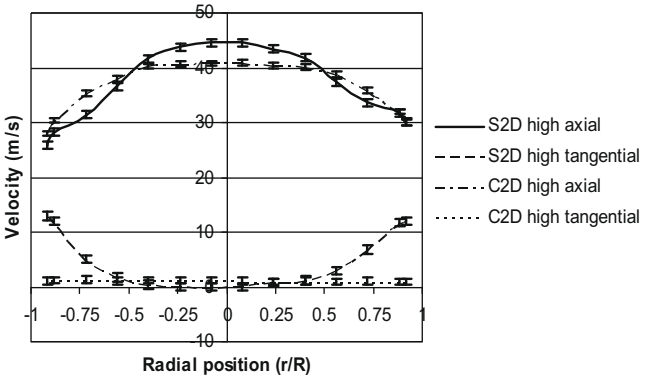

Fig. 7. Comparison of axial and tangential air velocity at the cross sectional horizontal line at a distance of two diameters downstream of the swirl and control pipe sections (all readings were taken across the horizontal diameter).

and swirl pipe sections for the three different Reynolds flow numbers. An analysis of these profiles concluded that the tangential velocity magnitude is zero at the wall, increases to its highest value in the shear region of the wall before decreasing to zero at the centre of the pipe. This profile is typically exhibited by swirl flows, more specifically by wall jet type of swirls.

Fig. 6 also shows that at a distance of two pipe diameters from the exit of the swirl pipe, the highest Reynolds number flow yields the highest tangential velocity, compared to the medium and low Reynolds number flows. As the measurement distance downstream of the swirl pipe outlet is increased, a decrease in the tangential velocity is observed. It was concluded from these graphs that the induced swirl decays with increasing distance downstream of the swirl pipe. Similarly the swirl can be said to decay faster for lower Reynolds number flows.

On the other hand, Fig. 6 shows that the tangential velocity generated downstream of the control pipe section exhibits a flat profile of magnitude that is almost non-existent, when compared to the tangential velocity from the swirl pipe.

In the high tangential velocity region close to the wall ($r/D = 0.9$) of Fig. 6, it is observed that the low Reynolds number flow flowing through the swirl pipe causes a higher tangential velocity at the furthest measured location than the high Reynolds number flow flowing through the control pipe at the closest measured location. It was concluded that the induced swirl has not completely decayed at a distance of fourteen diameters downstream of the swirl pipe.

Fig. 7 illustrates a graphical plot of the axial and tangential velocities measured along the pipe centreline at two pipe diameters downstream of the swirl or control pipe. An analysis of these plots concludes that velocities resulting from the swirl pipe are higher than those resulting from the control pipe. This is accompanied by the reverse effect closer to the pipe wall. On the other hand, the magnitude of tangential velocity as a result of the swirl pipe increases with radial distance from the pipe centre. It appears that the swirl pipe causes a redistribution of the velocities from axial to tangential, whereby energy shifts from axial momentum to angular momentum. This gives rise to a swirl component.

4. Determination of swirl numbers and decay rates

The degree of the swirl flow measured at each location may be quantified by the computation of the corresponding swirl number, as defined in Eq. (1). In order to obtain the swirl number for a specific plane, the ratio of the integrals of the functions, $u_\theta u_x r^2$ and $u_x^2 r$ over the area of the relevant measurement planes need to be evaluated. Since the exact values of the two functions are known at the

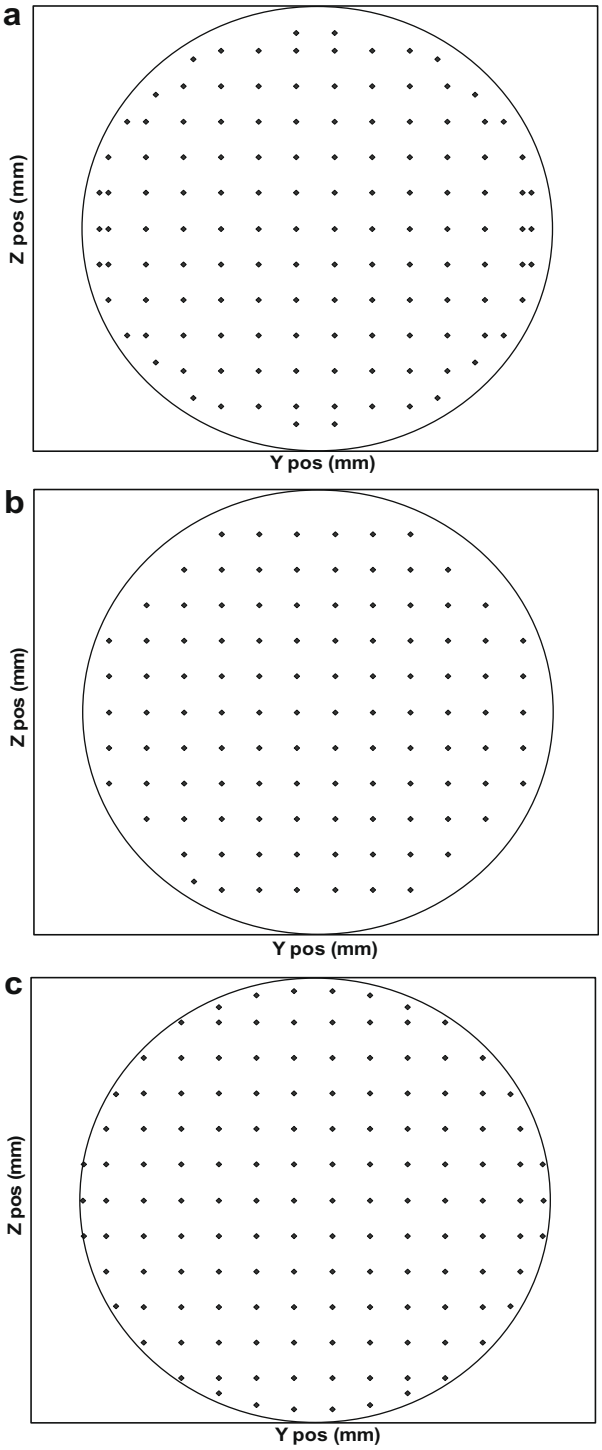

Fig. 8. (a) Matrix of measurement points in any y–z plane, (b) The original points post the deletion of 18 of the original points, (c) The final points including the 30 additional grid points.

measurement grid points, the numerical approximation scheme of straight summation was employed to compute the relevant integrals. That is, summing up the quotient of the function values and the approximate area of influence. Eq. (2) was interpreted as

$$S = \frac{\int (u_\theta u_x r^2) dA}{R \int (u_x^2 r) dA} = \frac{\sum_{i=1}^{n} (u_\theta u_x r^2) \partial A_i}{R \sum_{i=1}^{n} (u_x^2 r) \partial A_i} \tag{4}$$

To apply the equation to the measurement data, the area around each measurement location in the measurement plane, shown in Fig. 8a, was divided into smaller regular regions of influence. Eighteen measurement points close to the pipe wall had to be discarded in order to achieve a more regular grid Fig. 8b.

Eqs. (1) and (4) show that the integrand is proportional to r^2, which implies that the swirl number is significantly affected by the velocities near the wall. Inaccuracies in the swirl number estimation may occur because of the absence of velocity data in the region $0.92 < r/D < 1$. Thirty further grid points were added to minimise the error from any grid cell having too large an area of influence as shown in Fig. 8c. The value of the axial and tangential velocities at these 30 new points were estimated using the average result of linear interpolation between the last measurement point and the wall, where all velocities are zero, and linear extrapolation towards the wall of the line connecting the last two measurement points (Steenbergen and Voskamp, 1998).

The values of the resultant swirl numbers computed are presented in Fig. 9 and Table 4 for the three different Reynolds number flow regimes at 2, 6 and 10 pipe diameters downstream of the outlet to the swirl inducing pipe. Fig. 9 shows that the swirl number decreases with increasing distance downstream of the swirl pipe and that higher Reynolds number flows yields higher swirl numbers. This supports the conclusion that the swirl decays with respect to an increasing distance downstream of the swirl pipe exit and flows of decreasing Reynolds numbers.

To determine the decay rate for the three Reynolds number flows, an exponential regression function was fitted to the curves in Fig. 9, the exponential factor being divided by the pipe diameter (0.05 m). Table 5 summarises the values of the decay parameters determined for the swirl rate decay equations for each of the three Reynolds number flows. An analysis of the data collated from these experimental studies have confirmed that a three lobed helical pipe was able to generate a geometrically induced swirl with swirl numbers of 0.123, 0.144 and 0.151 at a distance of 2 pipe diameters downstream of the swirl inducing pipe for flows of Reynolds number 4.5×10^4, 9.0×10^4, and 1.4×10^5, respectively.

An examination of the behaviour predicted by these equations concluded that the swirl decays rapidly downstream of the swirl pipe, and further that the decay rates vary inversely with the Reynolds number of the flow. These findings therefore agree with those of Kreith and Sonju (1965), Baker and Sayre (1974) and Steenbergen and Voskamp (1998) who concluded that the decay rate is dependent on the initial conditions of the flow characterised by the Reynolds number.

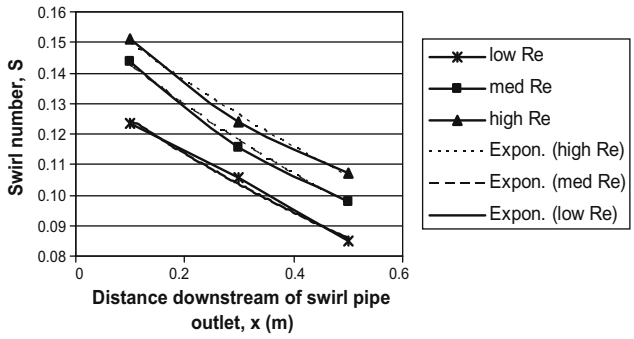

Fig. 9. Swirl numbers at planes 2, 6 and 10D downstream of swirl pipe for the low, medium and high Reynolds number flows.

Table 4
Swirl numbers at planes 2, 6 and 10D downstream of swirl pipe for the low, medium and high Reynolds number flows.

	S2D	S6D	S10D
Low *Re*	0.123	0.106	0.085
Med *Re*	0.144	0.116	0.098
High *Re*	0.151	0.124	0.107

Table 5
Swirl decay rates for the three Reynolds number flows.

Reynolds number flow	Swirl decay equation	Decay rate
High	$S = 0.1632e^{-0.8596x}$	17.19
Medium	$S = 0.1567e^{-0.9312x}$	18.62
Low	$S = 0.1368e^{-0.9569x}$	19.13

5. Conclusions

LDA was used for instantaneous velocity measurements. Analysis of contour plots created from the velocity data revealed that the three lobed helical pipe gave rise to a core triangular shaped contours downstream of the swirl pipe, compared to more circular contours downstream of the control pipe. The contour plots also confirmed the presence of a swirling flow from a shift in the orientation of the triangular contours with increasing distance downstream of the swirl pipe. It was also deduced that the flow was decaying as the orientation of the triangular contours was not offset by 360° over a distance equivalent to the pitch of the helical pipe, but occurred over a longer distance.

As expected, low velocity was observed closer to the wall and increasing to a maximum at the centre of the pipe for all three Reynolds number flows and for both the swirl inducing and the control pipe. The mean axial velocity was also shown to be increase with the Reynolds number of the flow, but inversely related to the distance downstream.

Contour plots of tangential velocity and the tangential velocity profile along the horizontal centreline of the pipe revealed that the tangential velocity was close to zero at the centre of the pipe with a sudden increase in the region $0.25 < r/D < 0.88$, before decreasing to zero again at the walls. The presence of wall jet swirls could be concluded from these profiles. The swirl pipe also caused a redistribution of the velocities from axial to tangential, whereby creating a transfer of momentum from axial to angular momentum. These effects were not observed with the control pipe.

The degree of the swirl component at each location was quantified using the swirl number. These confirmed the earlier conclusion that the swirl decays with respect to the flow Reynolds number and distance downstream of the swirl pipe. The swirl decay rates for the flows were calculated and it was found that they are inversely proportional to the Reynolds number of the flow.

The data presented in this paper documents this unique method of swirl generation, which is geometrically induced by the lobed cross-section of the pipe and the twist of this cross section. The significance of this finding is believed to be primarily valuable to lean phase pneumatic conveying, where there is often a need to locally increase the turbulent energy of the flow to reduce particle settlement and blockage, without escalating electricity costs. Swirl devices such as propeller type swirl generators, tangential slots, honeycomb structures, and inserts of twisted tapes, wires or tubes mounted at the inlet of the pipe have proved high maintenance as parts often detach themselves and they also cause blockage as the conveyed particles collect into them. The advantage of the swirl pipe over these swirl generation devices is that the swirl pipe is not intrusive to the flow and therefore avoids blockage which would otherwise occur and contains no moving parts. The swirl pipe is believed to be perfectly suited as the twist and lobes of

the swirl pipe produce centrifugal force which in turn increases average flow turbulence and promotes local secondary flows that prevent particle settlement.

Acknowledgements

The authors are indebted to Dr Matt Crompton, from Dantec Dynamics, for his support and assistance with the execution of the LDA experiments. The financial support from the University of Nottingham to undertake this research project is also gratefully acknowledged.

References

Algifri, A.H., Bhardwaj, R.K., 1985. Prediction of the heat transfer for decaying turbulent swirl flow in a tube. International Journal of Heat and Mass Transfer 28 (9), 1637–1643.

Algifri, A.H., Bhardwaj, R.K., Rao, Y.V.N., 1988. Turbulence measurements in decaying swirl flow in a pipe. Applied Scientific Research (The Hague) 45 (3), 233–250.

Baker D.W., Sayre, C.L., 1974. Decay of swirling turbulent flow of incompressible fluids in long pipes. In: Dowdell, R.B. (Ed.), Indus. Soc. of America, pp. 301–312.

Bali, T., 1998. Modelling of heat transfer and fluid flow for decaying swirl flow in a circular pipe. International Communications in Heat and Mass Transfer 25 (3), 349–358.

Bali, T., Ayhan, T., 1999. Experimental investigation of propeller type swirl generator for a circular pipe flow. International Communications in Heat and Mass Transfer 26 (1), 13–22.

Chang, F., Dhir, V.K., 1995. Mechanisms of heat transfer enhancement and slow decay of swirl in tubes using tangential injection. International Journal of Heat and Fluid Flow 16 (2), 78–87.

Chiu, C.L., Seman, J.J., 1971. Head loss in spiral solid–liquid flow in pipes. In: Zandi, I. (Ed.), Advances in Solid–Liquid Flow in Pipes and Its Applications, 1st ed. Pergamon Press Inc., Oxford, pp. 227–236.

Davis, J.C., 1986. Statistics and Data Analysis in Geology, second ed. John Wiley and Sons, New York.

Fokeer, S., Kingman, S., Lowndes, I., Reynolds, A., 2004. Characterisation of the cross sectional particle concentration distribution in horizontal dilute flow conveying – a review. Chemical Engineering and Processing 43 (6), 667–691.

Ganeshalingam, J., 2002. Swirl induction for improved solid–liquid flow in pipes. Ph.D. Thesis, University of Nottingham.

Hay, W., West, P.D., 1975. Heat transfer in free swirling flow in a pipe. Journal of Heat Transfer, Transactions ASME 97 (3), 411–416.

Herbreteau, C., Bouard, R., 2000. Experimental study of parameters which influence the energy minimum in horizontal gas–solid conveying. Powder Technology 112 (3), 213–220.

Jama, G.A., Klinzing, G.E., Rizk, F., 1999. Analysis of unstable behavior of pneumatic conveying systems. Particulate Science and Technology 17 (1–2), 43–68.

Kitoh, O., 1991. Experimental study of turbulent swirling flow in a straight pipe. Journal of Fluid Mechanics 225, 445–479.

Kreith, F., Sonju, O.K., 1965. The decay of a turbulent swirl in a pipe. Journal of Fluid Mechanics 22, 257–271.

Li, H., Tomita, Y., 1996. An experimental study of swirling flow pneumatic conveying system in a horizontal pipeline. ASME Journal of Fluids Engineering 118, 526–530.

Li, H., Tomita, Y., 1998. Numerical simulation of swirling gas–solid flow in a vertical pipeline. Particulate Science and Technology 19 (4), 355–368.

Li, H., Tomita, Y., 2000. Particle velocity and concentration characteristics in a horizontal dilute swirling flow pneumatic conveying. Powder Technology 107 (1–2), 144–152.

Li, H., Nozaki, T., Nakahori, K., 1999. An experimental study on a horizontal swirling flow pneumatic conveying with a curve pipe. In: Proceedings of the FEDSM.

Martemianov, S., Okulov, V.L., 2004. On heat transfer enhancement in swirl pipe flows. International Journal of Heat and Mass Transfer 47 (10–11), 2379–2393.

Narezhnyi, E.G., Sudarev, B.V., 1975. Calculation of the temperature of flame tubes of gas turbine combustion chambers with three-tier swirlers. Heat Transfer-Soviet Res. 6, 23–27.

Nejad, A.S., Vanka, S.P., Favaloro, S.C., Samimy, M., Langenfeld, C., 1989. Application of laser velocimetry for characterization of confined swirling flow. Journal of Engineering for Gas Turbines and Power 111, 36–45.

Nishibori, K., Koji, K., Mitsukiyo, M., Takeshi, M., 1987. Effect of inlet swirl on the turbulent flow in an axially rotating pipe. Transactions of JSME 53, 1150–1158.

Parchen, R.R., Steenbergen, W., 1998. An experimental and numerical study of turbulent swirling pipe flows. Journal of Fluids Engineering 120, 54–61.

Raylor, B., 1998. Pipe design for improved distribution and improved wear. Ph.D. Thesis, University of Nottingham.

Rocklage-Marliani, G., Schmidts, M., Ram, V.I.V., 2003. Three-dimensional Laser-Doppler Velocimeter measurements in swirling turbulent pipe flow. Flow Turbulence and Combustion 70, 43–67.

Spanner, E.F., 1945. Improvements in Tubes for Heat Exchanger Apparatus. GB569000 (patent).

Steenbergen, W., Voskamp, J., 1998. Rate of decay of swirl in turbulent pipe flow. Flow Measurement and Instrumentation 9 (2), 67–78.

Tashiro, H., Peng, X., Tomita, Y., 1997. Numerical prediction of saltation velocity for gas–solid two-phase flow in a horizontal pipe. Powder Technology 91 (2), 141–146.

Zaherzadeh, N.H., Jagadish, B.S., 1975. Heat transfer in decaying swirl flows. International Journal of Heat and Mass Transfer 18 (7–8), 941–944.